


Single-shot measurement of the space-varying polarization state of light through interferometric quantification of the geometric phase

Athira B S ^{1,*}, Mandira Pal,² Sounak Mukherjee,² Jatadhari Mishra,² Dibyendu Nandy ^{1,2} and Nirmalya Ghosh^{1,2}

¹*Center of Excellence in Space Sciences India, Indian Institute of Science Education and Research Kolkata, Mohanpur 741246, West Bengal, India*

²*Department of Physical Sciences, Indian Institute of Science Education and Research Kolkata, Mohanpur 741246, West Bengal, India*



(Received 28 May 2019; published 30 January 2020)

A light beam carrying a spatially varying state of polarization generates a space-varying Pancharatnam-Berry geometric phase while propagating through a homogeneous anisotropic medium. We show that determination of such a space-varying geometric phase provides a unique way to quantify the space-varying polarization state of light using a single-shot interferometric measurement. We demonstrate this concept in a Mach-Zehnder interferometric arrangement using a linearly polarized reference light beam, where full information on the spatially varying polarization state is successfully recovered by quantifying the space-varying geometric phase and the contrast of interference. The proposed method enables single-shot measurement of any space-varying polarization state of light from the measured interference pattern with a polarized reference beam. This approach shows considerable potential for instantaneous mapping of complex space-varying polarization of light in diverse applications, such as astronomy, biomedical imaging, and nanophotonics, where high precision and near real-time measurement of spatial polarization patterns are desirable.

DOI: [10.1103/PhysRevA.101.013836](https://doi.org/10.1103/PhysRevA.101.013836)

I. INTRODUCTION

Polarization measurement [1–3] has played an important role in our understanding of the complex structure of different biological samples [3], probing the dynamics of astrophysical phenomena [4,5], uncovering three-dimensional characteristics of chemical bonds [6], and for the characterization of complex nanomaterials and so forth [7]. Traditionally, polarization is measured using the four Stokes vector elements. This however involves multiple intensity measurements, which is not amenable to probing fast dynamical processes. Attempts have therefore been made to develop techniques that can instantaneously provide the full spatial polarization map, by simultaneously recording the different Stokes vector elements in multiple optical paths using combinations of polarizing beam splitters, retarders, etc. [8]. However, for applications involving polarization measurements with high spatial resolution and specifically for applications where the signal-to-noise ratio of polarization is weak, e.g., in solar coronal magnetometry [9], it is preferable to determine the space-varying polarization in a single optical path. This follows because division of light in multiple optical paths leads to further degradation of the signal-to-noise ratio. An alternative method is therefore highly sought for such applications.

The concept of the geometric phase and the associated spin-orbit interaction (SOI) of light may provide a route for this purpose. Note that the angular momentum carried by light can be divided into spin and orbital components, which are related to circular (elliptical) polarization [10] and

phase vortex [11,12] respectively. The spin and the orbital degrees of freedom of light can get coupled under certain circumstances, leading to interesting consequences such as SOI [13,14]. The SOI of light has attracted much attention due to its fundamental nature and potential applications in the development of spin photonic devices [7,15]. The SOI effect has an inherent geometrical origin that relates to the evolution of the geometric phase of light [15–19]. The topology of the evolution of the electromagnetic wave introduces two types of geometric phases [7,14,19–26]: (a) the spin redirection Berry phase, which arises when polarized light is passed through a twisted dielectric medium [14,23,25], and (b) the Pancharatnam-Berry phase, which arises due to continuous change in the polarization state of the wave when polarized light propagates through an anisotropic medium [7,19–24,26]. An interesting manifestation of SOI is the so-called spin Hall effect of light that leads to the spin- or circular-polarization-dependent splitting of the light beam and has been observed in various optical interactions [7,14,16,24]. The spin Hall effect is known to originate from the transverse (with respect to the direction of propagation) spatial or momentum gradient of either the Pancharatnam-Berry geometric phase or the spin redirection Berry phase [7,14,16]. For an incident homogeneously polarized light beam, the spin Hall effect produced in a transversely inhomogeneous anisotropic medium that arises due to the Pancharatnam-Berry geometric phase gradient is usually larger in magnitude as compared to those produced due to the spin redirection Berry phase in an isotropic medium, e.g., in tight focusing of fundamental or higher-order Gaussian beams, scattering from micro- and nanoscale systems, reflection, and refraction at dielectric interfaces [7,15,24,27].

*abs16rs013@iiserkol.ac.in

It is known that a light beam carrying inhomogeneous spatially varying polarization produces similar SOI effects due to the generation of the space-varying Pancharatnam-Berry geometric phase while propagating through a homogeneous anisotropic medium [24,28]. Thus, if any such spatially varying polarized light is passed through a homogeneous anisotropic medium, one can obtain information on the unknown space-varying polarization state through quantification of the space-varying geometric phase. In this paper we demonstrate this useful concept by developing a simple yet elegant interferometric technique for the quantification of the space-varying polarization state of light. Specifically, we concentrate on the single-shot determination of space-varying general elliptical polarization states because simultaneous retrieval of space-varying ellipticity and the orientation of a polarization ellipse is challenging and has numerous potential applications. For this purpose, we first demonstrate the manifestation of the space-varying geometric phase as spin-dependent splitting of a spatially varying polarized light beam while propagating through a homogeneous anisotropic medium. This lays the foundation for our next step, in which we quantify the spatially varying polarization of light in a Mach-Zehnder interferometric arrangement through quantification of the geometric phase and the interference contrast. The demonstrated principle of single-shot determination of spatially varying polarization states of light may find useful applications for mapping complex space-varying polarization patterns of remote light sources in diverse fields of physics ranging from nanophotonics [7] to materials characterization [6,29], biophotonics [3], and astronomy [4,5].

II. THEORY

When an inhomogeneously polarized or spatially varying polarized Gaussian beam propagates through a homogeneous anisotropic medium, it acquires a space-varying geometric phase. It can be shown that when such a spatially polarized Gaussian beam carrying a space-varying geometric phase is projected to right (RCP) or left circular polarization (LCP), it exhibits opposite momentum domain shifts of the centroid of the beam proportional to the spatial gradient of geometric phase (see Appendix A) [30]. Such a spin- or circular-polarization-dependent shift is similar to the momentum domain spin Hall effect of light [28,31,32]. In order to realize this phenomenon, we consider the case of a spatially varying polarized beam generated using a twisted nematic-liquid-crystal-based spatial light modulator (SLM). Here the symmetry of the polarization is broken along one of the transverse spatial coordinates ($\xi \rightarrow x/y$) of the beam. The evolution of polarization in the SLM can be modeled using the effective Jones matrix J_{eff} as a sequential product of matrices of an equivalent linear retarder J_{reta} (with effective linear retardance δ_{eff} and its orientation angle θ_{eff}) and an effective optical rotator R with optical rotation ψ_{eff} [31,32],

$$\begin{aligned} J_{\text{eff}} &= R(\psi_{\text{eff}})J_{\text{reta}}(\delta_{\text{eff}}, \theta_{\text{eff}}) \\ &= \begin{pmatrix} \cos \psi_{\text{eff}} & \sin \psi_{\text{eff}} \\ -\sin \psi_{\text{eff}} & \cos \psi_{\text{eff}} \end{pmatrix} \begin{pmatrix} \cos \theta_{\text{eff}} & -\sin \theta_{\text{eff}} \\ \sin \theta_{\text{eff}} & \cos \theta_{\text{eff}} \end{pmatrix} \\ &\quad \times \begin{pmatrix} e^{-i\delta_{\text{eff}}/2} & 0 \\ 0 & e^{i\delta_{\text{eff}}/2} \end{pmatrix} \begin{pmatrix} \cos \theta_{\text{eff}} & \sin \theta_{\text{eff}} \\ -\sin \theta_{\text{eff}} & \cos \theta_{\text{eff}} \end{pmatrix}, \quad (1) \end{aligned}$$

with $\psi_{\text{eff}} = -\psi + 2\theta_{\text{eff}}$. Here $\psi = \pi/2$ is the twist angle of the SLM. As is evident from Eq. (1), the state of polarization of light, i.e., the ellipticity, and the orientation angle of the polarization ellipse emerging from the SLM are determined by the polarization birefringence parameters δ_{eff} and ψ_{eff} . These parameters, in the individual SLM pixels, can be modulated by changing the gray level values n . Therefore, by modulating the pixels of the SLM using user-controlled gray level distributions, one can produce any desirable spatially varying polarization states of light using linearly polarized light as input. When such a spatially varying polarized light beam propagates through a homogeneous anisotropic medium (e.g., a half waveplate, whose fast axis is oriented at 45°) and is subsequently projected to the opposite-circular-polarization states, a space-varying geometric phase is generated.

Here the three relevant polarization states are

$$\begin{aligned} |A_{\text{SVP}}\rangle &= \begin{pmatrix} 1 \\ 0 \end{pmatrix}, \\ |B_{\text{SVP}}\rangle &= \begin{pmatrix} -i \sin \frac{\delta_{\text{eff}}(\xi)}{2} - \cos \frac{\delta_{\text{eff}}(\xi)}{2} \sin \psi_{\text{eff}}(\xi) \\ \cos \frac{\delta_{\text{eff}}(\xi)}{2} \cos \psi_{\text{eff}}(\xi) \end{pmatrix}, \\ |C\rangle &= \frac{1}{\sqrt{2}}(1 \pm i)^T, \end{aligned}$$

where $|A_{\text{SVP}}\rangle$ and $|B_{\text{SVP}}\rangle$ are, respectively, the input polarization state and the inhomogeneous spatially varying polarization state coming out of the half waveplate after passing through the SLM. The inhomogeneously polarized light coming out of the half waveplate is projected to the RCP state σ^+ or the LCP state σ^- , which is denoted by $|C\rangle$. The corresponding expression for the geometric phase that is acquired due to the evolution of polarization states can be obtained using the Pancharatnam connection as [32,33]

$$\phi_{\text{PB}}(\xi) = \arg(\langle A_{\text{SVP}}|C\rangle\langle C|B_{\text{SVP}}\rangle\langle B_{\text{SVP}}|A_{\text{SVP}}\rangle). \quad (2)$$

One can produce any desirable spatial gradient of the geometric phase by using an appropriate gradient of the gray levels ($\frac{dn}{d\xi=x/y}$) along a chosen linear direction ($\xi \rightarrow x/y$) of the SLM [32]. The resulting spatial gradient of the geometric phase manifests as shifts in the transverse momentum distribution ($\frac{k_{x/y}}{2\pi}$) in the Fourier domain of the Gaussian beam along the direction of the gradient, when projected to the RCP and LCP states (opposite shifts for RCP and LCP; see Appendix A). The corresponding momentum domain spin Hall shift ($\pm\Delta k_{x/y}$) can be quantified by detecting the shift of the centroid of the Gaussian momentum distribution [32]. Experimental demonstration of this concept is presented subsequently.

Having described the space-varying Pancharatnam-Berry geometric phase acquired by the spatially varying polarized light beam while propagating through a homogeneous anisotropic medium, we now turn to the quantification of the spatially varying polarization state through quantification of the geometric phase information. In general, the geometric phase depends upon the orientation of the polarization ellipse with respect to the anisotropy axis of the homogeneous anisotropic medium [15,17,26]. Moreover, if the transmitted spatially varying polarized light beam is made to interfere

with a linearly polarized reference beam, the information on the polarization ellipticity and the orientation of the polarization ellipse will also be encoded in the spatially varying contrast of the interference. Therefore, in principle, the geometric phase and the contrast information can be combined to obtain complete information on the space-varying elliptical polarization (ellipticity and orientation of the ellipse) using interferometric measurement with appropriate calibration of the dynamical phase of the interferometer. In order to experimentally demonstrate this concept, we take the example of the symmetry-broken spatially varying polarized light beam generated by the SLM, described above. Note that, unlike the previous case, the state $|C\rangle$ is not required here for retrieval of space-varying polarization using interferometric determination of the space-varying geometric phase of light. For this specific interferometric arrangement, the space-varying geometric phase is acquired in one arm of the interferometer due to the propagation of the spatially varying polarized state generated by the SLM through the homogeneous anisotropic medium or the half waveplate and subsequent evolution of the state to $|B_{SVP}\rangle$. The corresponding expression for the geometric phase is then given by

$$\phi_{PB}(\xi) = \arg(\langle A_{SVP} | B_{SVP} \rangle) = \tan^{-1} \left(\frac{\tan \frac{\delta_{\text{eff}}(\xi)}{2}}{\sin \psi_{\text{eff}}(\xi)} \right). \quad (3)$$

As is evident, in this case, the generated space-varying geometric phase depends upon the spatial distribution of the $\delta_{\text{eff}}(\xi)$ and $\psi_{\text{eff}}(\xi)$ birefringence parameters of the SLM. The space-varying polarization state to be reconstructed (which is generated using the SLM) is also determined by these polarization birefringence parameters. Thus, our job here is to determine the $\delta_{\text{eff}}(\xi)$ and $\psi_{\text{eff}}(\xi)$ birefringence parameters through interferometric quantification of the geometric phase of light, which can then be subsequently used to retrieve the space-varying polarization of the light beam. Note that, in principle, any arbitrary space-varying polarization state coming from a distant source can be determined using this approach by quantifying the ellipticity and orientation of the polarization ellipse through interferometric quantification of the geometric phase information with proper calibration of the dynamical phase of the interferometer.

It can be seen from Eq. (3) that the geometric phase expression has two composite parameters $\delta_{\text{eff}}(\xi)$ and $\psi_{\text{eff}}(\xi)$; however, that alone does not allow us to quantify them separately. As previously noted, since the reference light beam of the interferometer is linearly polarized, the orientation of the polarization ellipse in the sample interference arm [which is also determined by the $\delta_{\text{eff}}(\xi)$ and $\psi_{\text{eff}}(\xi)$ birefringence parameters] will affect the contrast of interference. So, with an extra measurement of contrast along with the geometric phase information, one can extract both the space-varying polarization parameters $\delta_{\text{eff}}(\xi)$ and $\psi_{\text{eff}}(\xi)$ and subsequently retrieve the space-varying polarization. In order to accomplish this, we proceed as follows. (i) We first determine the space-varying Pancharatnam-Berry geometric phase from the interference pattern in a Mach-Zehnder configuration with appropriate calibration of the dynamical phase of the interferometric system. (ii) We then quantify the spatially varying contrast of the interference fringe. The birefringence parameters are

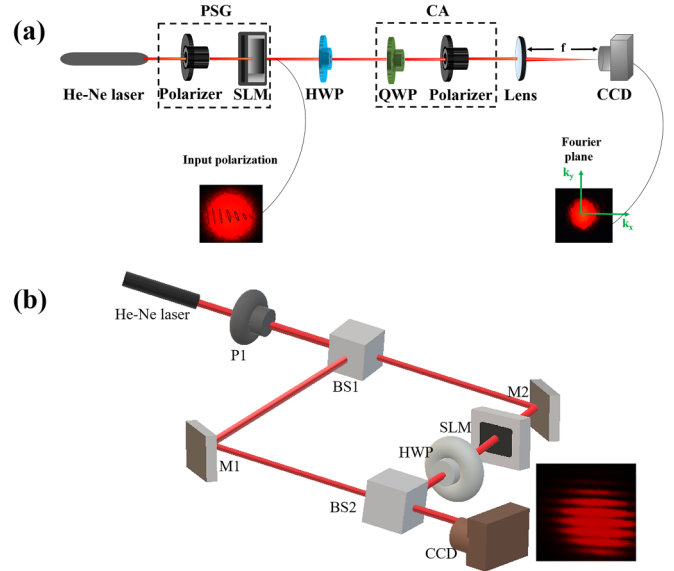


FIG. 1. (a) Schematic of the experimental arrangement for observing spin-dependent splitting of a spatially varying polarized light beam in a homogeneous anisotropic medium. The polarization state generator (PSG) unit comprises a linear polarizer followed by a spatial light modulator (SLM). A half waveplate (HWP) is used as the homogeneous anisotropic medium. To observe the spin-dependent splitting of light, the transmitted beam was analyzed via the circular analyzer (CA) comprising a rotatable quarter waveplate (QWP) followed by a linear polarizer. (b) Mach-Zehnder interferometric arrangement for quantification of the space-varying polarization state of light: P1, polarizer; BS1 and BS2, beam splitters; M1 and M2, mirrors; and HWP, half waveplate.

extracted using suitable calibration of the dependence of the contrast on these polarization parameters of the SLM. This information is subsequently used to retrieve the spatially varying polarization state of light generated by the SLM.

III. EXPERIMENTAL METHODS

A schematic of the experimental arrangement for observing the spin-dependent splitting of the spatially varying polarized light beam is shown in Fig. 1(a). A fundamental Gaussian mode of the 632.8 nm line of a He-Ne laser is used to seed the system. The spatially varying polarized beam is generated using the polarization state generator unit, which comprises a fixed linear polarizer (P1) and a transmissive SLM. A gray level gradient ($\frac{dn}{d\xi=x/y} = 0.0653 \text{ bit}/\mu\text{m}$) was created in the SLM pixels along one chosen linear direction ($\xi \rightarrow x/y$) using a range of gray level values between $n = 40$ and 90 . This choice was driven by the observed linear variations of the $\delta_{\text{eff}}(n)$ and $\psi_{\text{eff}}(n)$ parameters over this range of n values [32]. The beam is then passed through a half waveplate, which acts as the homogeneous anisotropic medium. The transmitted light beam is then sequentially analyzed for RCP and LCP basis states by projecting it to opposite circular analyzers. The circular analyzer comprises a rotatable quarter waveplate and a linear polarizer. The beam transmitted through the circular analyzer was imaged into a CCD camera. The CCD camera was placed at the back focal Fourier plane of the Fourier

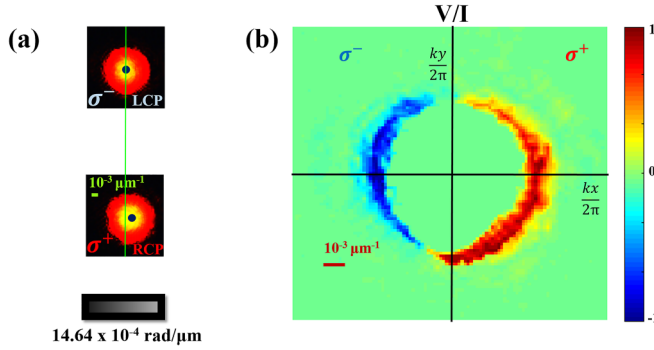


FIG. 2. Manifestation of the space-varying Pancharatnam-Berry geometric phase as spin-dependent splitting of the spatially varying polarized beam in a homogeneous anisotropic medium. (a) Transverse momentum distributions ($\frac{k_{x/y}}{2\pi} \mu\text{m}^{-1}$) of the transmitted beam for the symmetry-broken spatially varying polarized beam. Opposite shifts in the transverse momentum distribution of the LCP (σ^- , top panel) and RCP (σ^+ , middle panel) analyzed symmetry-broken spatially varying polarized beam are observed. A gray level gradient was applied along the x direction in the SLM and the applied gray level values ($n = 40-90$) are displayed (bottom panel). (b) Corresponding distribution of the Stokes vector element V/I .

transforming lens with focal length f . In this configuration, the recorded intensity distribution at the CCD (x', y') plane (Fourier plane) represented the transverse momentum (spatial frequency) distribution [$\frac{k_x}{2\pi} = \frac{x'}{\lambda f}$; $\frac{k_y}{2\pi} = \frac{y'}{\lambda f}$]. The momentum domain spin Hall shift was quantified by determining the shift in the centroid of the transverse momentum distribution ($\frac{k_{x/y}}{2\pi}$) between the RCP and the LCP projections.

The Mach-Zehnder interferometric arrangement for the quantification of space-varying polarization is shown in Fig. 1(b). The spatially varying polarized light beam generated by the SLM is used in one arm of the interferometer and a horizontally polarized Gaussian beam is used as the reference beam in the other arm. The interference pattern is captured using a CCD camera.

IV. RESULTS AND DISCUSSION

A. Spin-dependent splitting of a spatially varying polarized light beam in a homogeneous anisotropic medium

Making use of the experimental arrangement [Fig. 1(a)], spin-dependent splitting of the transverse momentum distribution ($\frac{k_{x/y}}{2\pi} \mu\text{m}^{-1}$) of the spatially varying polarized beam is demonstrated in Fig. 2. Note that, before recording the spin-dependent splitting of the spatially varying polarized light (using the gray level gradient in the SLM), measurements were taken by giving a uniform gray level distribution in the SLM. No shift in the centroid of the Gaussian beam was recorded when the output beam was projected to RCP and LCP states by rotating the quarter waveplate at the detection end. Taking this measurement as a reference, similar measurements were subsequently performed on spatially varying polarized light by applying the desirable gray level gradient in the SLM. The projected LCP mode σ^- (top panel) and the RCP mode σ^+ (bottom panel) experience opposite momentum domain shifts, observed as a shift of the beam centroid in the detection plane

[Fig. 2(a)]. This manifests as a spin separation or spatially separated regions of opposite-circular-polarization states in the circular-polarization descriptor Stokes vector element $\frac{V}{I}$ ($= \frac{I_{\text{RCP}} - I_{\text{LCP}}}{I_{\text{RCP}} + I_{\text{LCP}}}$) [Fig. 2(b)]. The spin- or circular-polarization-dependent momentum domain beam shift corresponding to our experimental configuration was estimated theoretically using Eqs. (A1) and (A2). The experimentally observed shift of the centroid of the Gaussian momentum distribution in the Fourier plane ($\frac{\Delta k_{x/y}}{2\pi} \sim \pm 13.68 \times 10^{-4} \mu\text{m}^{-1}$) is found to be in excellent agreement with the theoretically calculated momentum domain shift ($\pm 14.64 \times 10^{-4} \mu\text{m}^{-1}$). These results provide evidence that the spatially varying polarized light beam generates a space-varying geometric phase while propagating through a homogeneous anisotropic medium, quantification of which opens up an interesting avenue for the determination of any space-varying polarization state of light.

B. Interferometric determination of space-varying polarization

Figure 3 summarizes the results of quantification of space-varying polarization through quantification of Pancharatnam-Berry geometric phase using the Mach-Zehnder interferometric arrangement [Fig. 1(b)]. A homogeneously polarized light beam generated by applying a uniform gray level distribution at the SLM was first used in the sample arm to calibrate the dynamical phase of the interferometric arrangement. Interference patterns with a linearly polarized reference beam were sequentially recorded using both the homogeneously polarized and the spatially varying polarized light beam passing through the half waveplate. The spatial variation of the phase at the CCD plane was subsequently quantified using the conventional Fourier transform method along with the phase unwrapping procedure [34–36]. Figure 3 displays the extracted unwrapped dynamical phase of the interferometer corresponding to the homogeneously polarized light beam [Fig. 3(a)], the unwrapped total phase (dynamical plus geometric phase) corresponding to the spatially varying polarized light beam [Fig. 3(b)], and the geometric phase [Fig. 3(c)] that is exclusively related to the spatially varying polarization state of light. As anticipated, the extracted geometric phase exhibits a spatial gradient along the direction (y) of the gray level gradient in the SLM. Figure 3(d) shows the calibration of interference contrast with varying optical rotation parameter $\psi_{\text{eff}}(n)$ of the SLM for different sets of homogeneously polarized beams (varying from $n = 40$ to 90). Since the circular birefringence or the optical rotation parameter ψ_{eff} determines the orientation of the polarization ellipse in the sample arm of the interferometer, increasing the magnitude of ψ_{eff} with respect to the linear polarization state that is used in the reference arm will degrade the contrast of interference. This calibration curve is subsequently utilized to quantify the spatial (y) variation of the ψ_{eff} parameter [Fig. 3(e)] from the spatially varying contrast of interference [top panel of Fig. 3(e) and inset]. Once the $\psi_{\text{eff}}(y)$ parameter is determined, the extracted spatial variation of the geometric phase [Fig. 3(c)] yields the spatial variation of the other polarization birefringence parameter, the linear retardance δ_{eff} of the SLM using Eq. (3) [shown in Fig. 3(f)].

As previously noted, the controlled inputs δ_{eff} and ψ_{eff} , the birefringence parameters of the SLM, contain information on

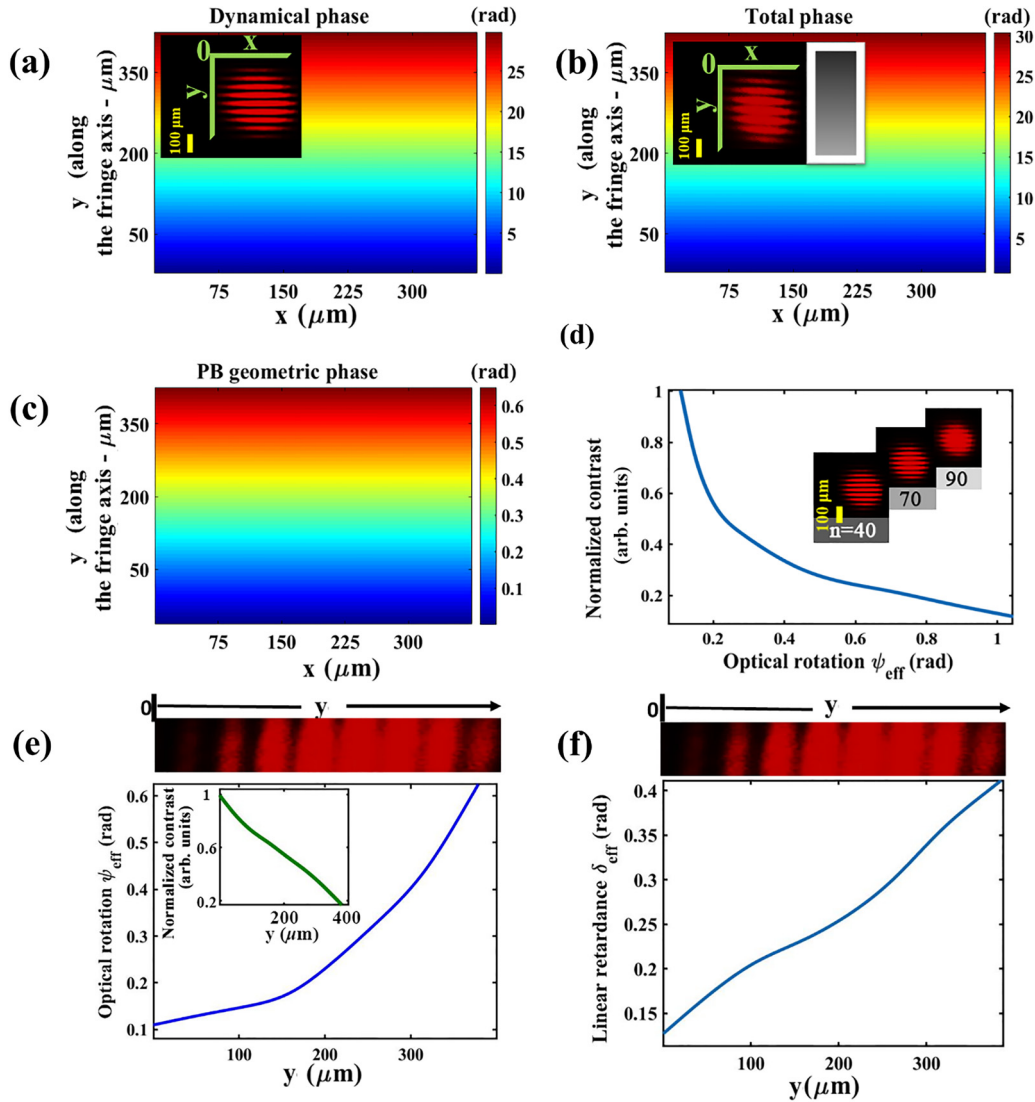


FIG. 3. Interferometric determination of space-varying polarization through quantification of the Pancharatnam-Berry geometric phase. (a) Dynamical phase of the interferometer extracted from the interference fringes (shown in the inset) corresponding to a homogeneously polarized light beam. (b) Total phase and (c) geometric phase extracted from the interference fringe (shown in the inset) corresponding to the spatially varying polarized beam. (d) Dependence of the contrast of interference on the varying optical rotation parameter ψ_{eff} of the SLM obtained by changing the gray level values ($n = 40-90$) for different sets of homogeneously polarized beams. The inset shows the corresponding interference patterns for different n . (e) Spatial (y) variation of ψ_{eff} derived from the spatially varying contrast [corresponding to the fringe shown in the top panel of (e)] when the spatially varying polarized beam is used. The inset shows the corresponding spatial (y) dependence of the contrast. (f) Derived spatial variation of the linear retardance parameter $\delta_{\text{eff}}(y)$ of the SLM for the spatially varying polarized beam.

the ellipticity and the orientation angle of polarization ellipse, respectively, of the polarization state generated by the SLM. Therefore, the retrieved spatial variation of the $\delta_{\text{eff}}(y)$ and $\psi_{\text{eff}}(y)$ parameters are used to determine the spatially varying polarization state of the light beam generated by the SLM. The corresponding results are summarized in Fig. 4. The retrieved spatial variation of the polarization birefringence parameters δ_{eff} and ψ_{eff} and the recovered spatially varying polarization state show excellent agreement with the controlled input parameters [Fig. 4(a)] and the corresponding spatially varying polarization state generated by the SLM [Fig. 4(b)], respectively. In order to further comprehend these experimental results, we present in Appendix B (Fig. 5) a simulation of

all the above steps of the experiment involving interferometric determination of the geometric phase and the dynamical phase of light for subsequent retrieval of space-varying polarization. The presented experimental results and the corresponding results of the simulations clearly demonstrate the ability of the proposed technique for the quantification of the space-varying polarization state of light through quantification of the space-varying Pancharatnam-Berry geometric phase using a single-shot interferometric measurement. The principle has been demonstrated for the general case of space-varying elliptical polarization and thus it is equally applicable for space-varying linear polarization states as well. As an example, simulation results of this approach for retrieving the radially

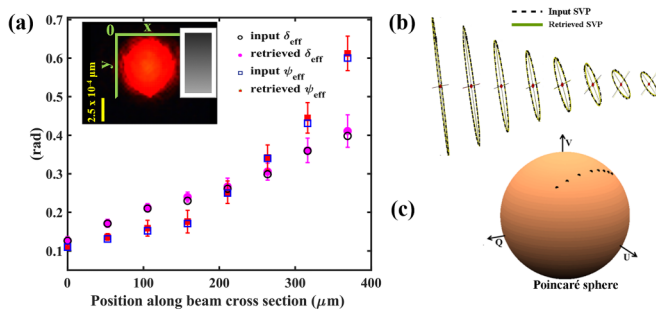


FIG. 4. Comparison of the retrieved space-varying polarization state using the interferometric measurement with the controlled input. (a) Spatial (y) variation of the derived (closed symbols) polarization birefringence parameters $\delta_{\text{eff}}(y)$ (circles) and $\psi_{\text{eff}}(y)$ (squares) and the corresponding controlled inputs (open symbols) in the SLM. (b) Corresponding retrieved spatially varying polarization states (solid line) and the controlled input states (dashed line) at the SLM. (c) Poincaré sphere representation of the retrieved spatially varying polarization states.

polarized vector beam are shown in Appendix C (Fig. 6). However, retrieval of space-varying pure linear polarization is less challenging in general and can be achieved using other simpler approaches also.

We emphasize that in this particular scenario of the space-varying polarization state generated by an SLM, the demonstrated interferometric determination of the $\delta_{\text{eff}}(\xi \rightarrow x/y)$ and $\psi_{\text{eff}}(\xi \rightarrow x/y)$ parameters is equivalent to determination of the space-varying ellipticity and orientation of the polarization ellipse for the general case of any spatially varying polarized light from remote sources. Moreover, in this specific case, since the space-varying polarization state was generated by introducing the SLM in one arm of the interferometer, it necessitated cumbersome calibration of the dependence of the contrast on the birefringence parameters of the SLM [shown in Fig. 3(d)]. This may not be needed for the general case, where the extracted spatial variation of the geometric phase and the interference contrast contain sufficient information to retrieve complete information on the spatial variation of the polarization. Although the principle has been demonstrated for completely polarized light, it can also be extended to incorporate partial polarization states by including additional calibration of the dependence of the contrast of interference on the degree of polarization of light.

V. CONCLUSION

In summary, we have demonstrated an experimental technique for the quantification of the space-varying polarization state of light using a single-shot interferometric measurement. This method is based on the determination of the space-varying Pancharatnam-Berry geometric phase that a spatially varying polarized light generates while propagating through a homogeneous anisotropic medium. It was shown that the information on the space-varying geometric phase and the space-varying contrast of the interference obtained using a polarized reference light beam can be combined to yield complete information on the spatially varying polarized light. This principle was experimentally demonstrated in a Mach-

Zehnder interferometric arrangement by recovering spatially varying polarized light generated by a spatial light modulator. With regard to the accuracy and sensitivity of the method, we would like to note that the sensitivity and accuracy of the determination of space-varying polarization is entirely determined by the sensitivity of the interferometric setup for the quantification of the phase. Since this method is based on quantification of the phase through interferometry, it is expected to yield better sensitivity as compared to the traditional intensity-based polarization measurement methods [1–3]. This, however, remains to be rigorously evaluated. This single-shot interferometric polarimetry technique may significantly enhance polarimetric applications for probing the dynamics of a wide range of phenomena in diverse systems ranging from complex materials [6,29] and biological systems [3] to the astrophysical domain [4,5], where high cadence and high precision measurement of spatial polarization patterns are desirable [9]. Finally, the proposed interferometric approach for spatially varying polarization measurements represents a fundamentally interesting approach with much potential. The expansion of our investigation toward practical applications is left for future work.

ACKNOWLEDGMENTS

The authors acknowledge the Indian Institute of Science Education and Research Kolkata for funding and facilities. A.B.S. is grateful to Ministry of Human Resources Development, Government of India, for a research fellowship through Center of Excellence in Space Sciences India. M.P., S.M., and J.M. acknowledge funding from the INSPIRE program of the Department of Science and Technology, INSPIRE, Government of India.

APPENDIX A: SPIN-DEPENDENT SPLITTING OF A SPATIALLY VARYING POLARIZED LIGHT BEAM IN A HOMOGENEOUS ANISOTROPIC MEDIUM

The experimental results for the spin-dependent splitting of spatially varying polarized light are presented above. Here we discuss the underlying physical mechanism. A Gaussian beam with a spatially varying polarization state propagating along the z direction of a homogeneous anisotropic medium acquires a space-varying Pancharatnam-Berry (PB) geometric phase [24,30]. If a constant spatial gradient of this geometric phase is generated ($\frac{d\phi_{\text{PB}}}{d\xi} = \Omega_{\xi}; \xi \rightarrow x/y$), it will lead to a shift in the distribution of transverse momentum ($\pm \frac{\Delta k_x/y}{2\pi}$) of the Gaussian beam along the direction of the gradient, when projected to RCP and LCP states. This momentum domain spin Hall shift can be quantified by as a shift of the beam centroid of the Gaussian beam in the detection Fourier plane [32]. In our case, the input inhomogeneous polarization state is generated using a twisted nematic-liquid-crystal-based SLM. The polarization response of the SLM can be modeled as a product of Jones matrices of an equivalent linear retarder and an optical rotator [Eq. (1)] with effective linear retardance δ_{eff} and effective optical rotation ψ_{eff} . Since these polarization birefringence parameters can be controlled by changing the gray level values n in the SLM, one can controllably generate the spatially polarized beam. The dependence of δ_{eff} and ψ_{eff} on the

gray level n for our SLM was determined in our previous publication [32], which has been used here to generate the desired spatial variation of the polarization state. Thus, one can produce an inhomogeneous spatially polarized light beam creating a gray level gradient ($\frac{dn}{d\xi=x/y}$) in the SLM along one chosen linear direction (x or y). The input inhomogeneously polarized light then passes through a half waveplate, oriented at 45° with respect to the horizontal of the laboratory frame, giving an inhomogeneous polarization state $|B_{\text{SVP}}\rangle$,

and is then subsequently projected to the circular-polarization state $|C\rangle$.

The expression for the geometric phase that is generated due to this polarization evolution can be determined from Eq. (2) by using the expression of the states $|A_{\text{SVP}}\rangle$, $|B_{\text{SVP}}\rangle$, and $|C\rangle$ as the space-varying polarization state coming out of the SLM, the space-varying polarization state coming out of half waveplate, and projecting onto a circular polarizer, respectively:

$$\phi_{\text{PB}}(\xi) = \tan^{-1} \left(\frac{\cos^2 \frac{\delta_{\text{eff}}(\xi)}{2} \cos \psi_{\text{eff}}(\xi) \sin \psi_{\text{eff}}(\xi) (2 \cos^2 \frac{\delta_{\text{eff}}(\xi)}{2} \cos^2 \psi_{\text{eff}}(\xi) - 1)}{2 \cos^4 \frac{\delta_{\text{eff}}(\xi)}{2} \cos^2 \psi_{\text{eff}}(\xi) [1 - \cos^2 \psi_{\text{eff}}(\xi)]} \right). \quad (\text{A1})$$

By applying a gray level gradient for the chosen range of n values (for $n = 40-90$) where the parameters ψ_{eff} and the δ_{eff} exhibit an approximate linear dependence [Fig. 3(c) of Ref. [32]], a desirable spatial gradient of the geometric phase (Ω_ξ) was generated. This resulted in the shift of the transverse momentum distribution of the Gaussian beam for the RCP and LCP projection states as

$$\frac{\Delta k_{x/y}}{2\pi} = \pm \Omega_\xi. \quad (\text{A2})$$

For the applied gray level gradient $\frac{dn}{d\xi=x/y} = 0.0653 \text{ bit}/\mu\text{m}$, the momentum domain spin Hall shift for our experimental case was determined using Eqs. (A1) and (A2) to be $\frac{\Delta k_{x/y}}{2\pi} \sim \pm 14.64 \times 10^{-4} \mu\text{m}^{-1}$.

APPENDIX B: SIMULATION OF INTERFEROMETRIC DETERMINATION OF SPACE-VARYING POLARIZATION

The experimental setup and the results for quantifying a space-varying polarization state from interferometric measurement have been discussed in Secs. III and IV B. Here we provide stepwise procedures of numerical simulation of the experiment involving interferometric determination of the geometric phase and dynamical phase of light for subsequent retrieval of space-varying polarization. The necessary equations used in the simulation are outlined.

In order to generate a spatially varying polarization along the y direction (in Fig. 3), we used the SLM in one arm of the interferometer. This was followed by a half waveplate acting as the homogeneous anisotropic medium, with its fast axis at 45° with respect to the horizontal. The electric fields of the initially horizontally polarized (Jones vector $[1 \ 0]^T$) Gaussian beam coming out of the sample arm and from the reference arm can be written as

$$\begin{aligned} \mathbf{E}_1 &= e^{-(x^2+y^2)/\omega_0^2} \begin{pmatrix} 0 & 1 \\ 1 & 0 \end{pmatrix} J_{\text{eff}} \begin{pmatrix} 1 \\ 0 \end{pmatrix}, \\ \mathbf{E}_2 &= e^{-(x^2+y^2)/\omega_0^2} \begin{pmatrix} 1 \\ 0 \end{pmatrix}. \end{aligned} \quad (\text{B1})$$

Here J_{eff} is the Jones matrix of the SLM [Eq. (1)]. For the sake of simplicity, we have considered a simple Gaussian spatial electric field profile of the beam, where x and y are the transverse spatial coordinates and ω_0 is the spot size of the

beam. Here \mathbf{E}_1 is the electric field from the path containing the SLM and half waveplate, whereas \mathbf{E}_2 is the horizontally polarized electric field from the other arm. In order to simulate the experimental interference fringe, we consider that \mathbf{E}_1 acquires a dynamical phase αy relative to \mathbf{E}_2 due to the path difference in the interferometer (α is the gradient of the dynamical phase along y). The resultant electric field that is used to simulate the interference pattern can be written as

$$\mathbf{E} = \mathbf{E}_1 e^{i\alpha y} + \mathbf{E}_2. \quad (\text{B2})$$

The simulations are performed using the input parameters $\alpha = 0.075 \text{ rad } \mu\text{m}^{-1}$ and $\omega_0 = 300 \mu\text{m}$. Figure 5 summarizes the results of the simulation corresponding to the experimental results presented in Fig. 3. Figure 5(a) shows the interference fringe corresponding to a homogeneously polarized light beam (with no spatial variation of the gray level imparted in the SLM). The corresponding spatial phase pattern is solely the dynamical phase of the interferometer ($\sim \alpha y$). Figure 5(b) shows the simulation results for the spatially varying polarized light [with spatial variation of the gray level imparted in the SLM, modeled by using the corresponding $\delta_{\text{eff}}(n)$ and $\psi_{\text{eff}}(n)$ parameters in J_{eff} of Eq. (B1)]. The corresponding spatial phase pattern has contributions from both the spatially varying dynamical phase of the interferometer and the spatially varying geometric phase that is related to the space-varying polarization. The spatial variation of the geometric phase is subsequently extracted by subtracting the phase pattern of Fig. 5(a) from that of Fig. 5(b) and is shown in Fig. 5(c).

Like the case of the experimental contrast calibration [Fig. 3(d)], here also the interference patterns are simulated for homogeneous polarization states generated by the SLM using different uniform gray level values ($n = 40-90$) by using the corresponding SLM Jones matrices J_{eff} in Eqs. (B1) and (B2). As noted in this paper, the contrast is primarily determined by the optical rotation parameter ψ_{eff} which determines the orientation of the polarization ellipse. Accordingly, the variation of the normalized contrast ($\frac{I_{\text{max}} - I_{\text{min}}}{I_{\text{max}} + I_{\text{min}}}$) with the varying parameter ψ_{eff} is shown in Fig. 5(d), which is subsequently used as the contrast calibration curve. Now, for the case of spatially varying polarization, the contrast of the simulated fringes varies along y due to the variation of the parameter ψ_{eff} along y . The normalized contrast is locally calculated for different points along the y direction, which is then used to determine the spatial variation of the parameter $\psi_{\text{eff}}(y)$ using

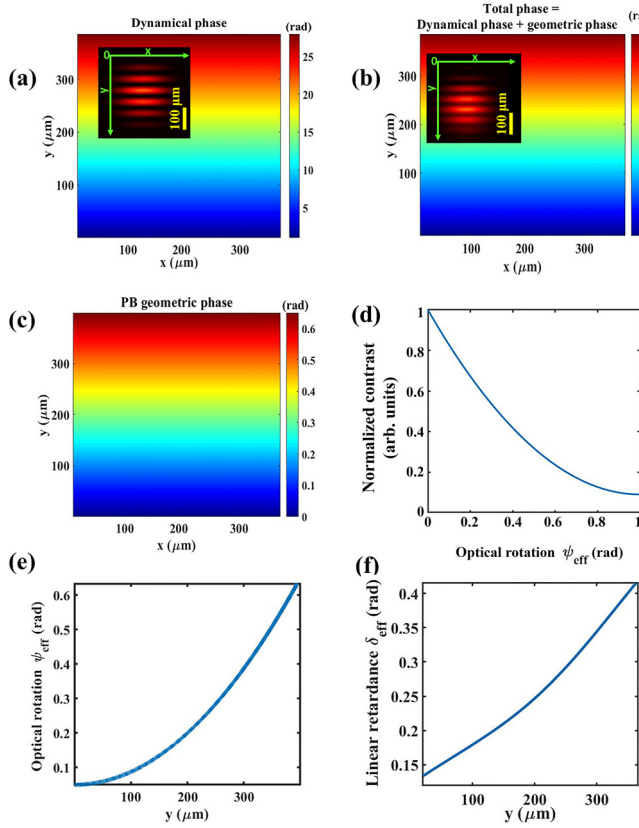


FIG. 5. Numerical simulation of interferometric determination of space-varying polarization. (a) Simulated interference fringe (shown in the inset) corresponding to a homogeneously polarized light beam by utilizing the dynamical phase corresponding to the experiment. (b) Total phase and (c) PB geometric phase extracted from the simulated interference fringe (shown in the inset) corresponding to the light beam with spatially varying polarization. (d) Dependence of the contrast of interference on the varying optical rotation parameter ψ_{eff} of the SLM obtained by changing the gray level values ($n = 40-90$) for different sets of homogeneously polarized beams. (e) Spatial (y) variation of the parameter derived from the spatially varying contrast (corresponding to the fringe shown in the top panel) when the spatially varying polarized light beam is used. (f) Derived spatial variation of the linear retardance parameter $\delta_{\text{eff}}(y)$ of the SLM for the SVP beam.

the calibration curve of Fig. 5(d). The corresponding variation of $\psi_{\text{eff}}(y)$ is shown in Fig. 5(e). The spatial variation of the linear retardance parameter $\delta_{\text{eff}}(y)$ is subsequently obtained from the spatial variation of the geometric phase in Fig. 5(c) using $\psi_{\text{eff}}(y)$ and Eq. (3). The corresponding result is shown in Fig. 5(f). Once the parameters $\delta_{\text{eff}}(y)$ and $\psi_{\text{eff}}(y)$ are determined from the interference patterns, these are used to retrieve the space-varying polarization state generated by the SLM.

The simulation results presented above confirm the experimental results presented in Fig. 3. The important trends are observed to be similar. The dependence of the contrast of interference on the optical rotation parameter ψ_{eff} and the spatial (y) dependence of both the $\psi_{\text{eff}}(y)$ and the $\delta_{\text{eff}}(y)$ parameters are observed to be in good agreement, thus establishing the self-consistency of the method.

APPENDIX C: MAPPING OF A RADIAL POLARIZATION STATE OF LIGHT USING THE INTERFEROMETRIC SINGLE-SHOT MEASUREMENT SCHEME

The proposed method has been demonstrated for space-varying elliptical polarization. It is equally applicable for any space-varying linear polarization states as well. Here we provide an illustrative example of a numerical simulation for recovering a two-dimensional space-varying linear polarization state of light i.e., for a radially polarized vector beam. The state of radial polarization can be conveniently described using the Jones vector $[\cos \varphi \ \sin \varphi]^T$, where φ is the azimuthal angle. Recovery of such space-varying pure linear polarization is less challenging as compared to the general space-varying elliptical polarization, as one would only need to map the φ dependence of the orientation of the polarization vector.

In order to implement the geometric phase principle of our proposed method, we propagate the radially polarized beam through a quarter waveplate oriented at 45° with respect to the horizontal axis followed by a linear polarizer (oriented vertically) in one of the arms of a Mach-Zehnder interferometer by which it acquires the space-varying PB geometric phase [see Eq. (C1)]. It then interferes with a reference vertical linear polarization state ($[0 \ 1]^T$). The evolution of the polarization state in the sample arm and the acquired geometric phase can be modeled as

$$|A\rangle = \begin{pmatrix} \cos \varphi \\ \sin \varphi \end{pmatrix}, \quad |B\rangle = \frac{1}{\sqrt{2}} \begin{pmatrix} 0 \\ \sin \varphi - i \cos \varphi \end{pmatrix},$$

$$\phi_{\text{PB}} = \arg(\langle A|B\rangle) = \tan^{-1}(-\cot \varphi). \quad (\text{C1})$$

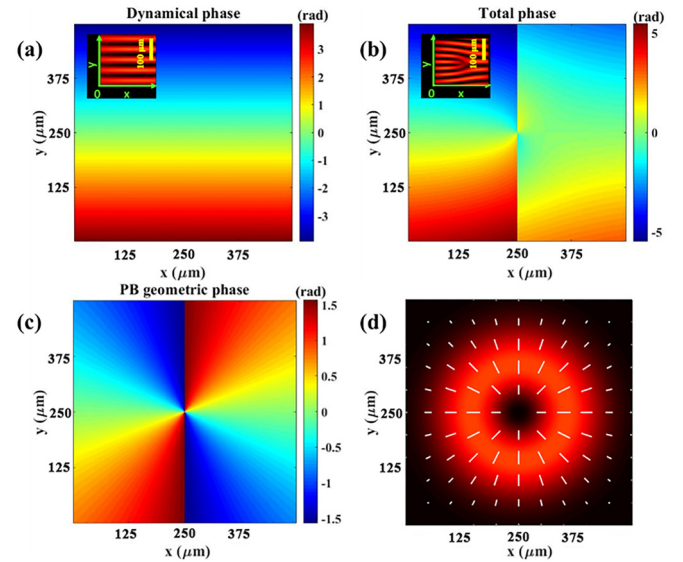


FIG. 6. Numerical simulation for extraction of the two-dimensional spatial polarization distribution for a radially polarized vortex beam. (a) Applied dynamical phase for simulating the interference fringes (shown in the inset) corresponding to a homogeneously polarized Gaussian beam. (b) Total phase and (c) PB geometric phase extracted from the simulated interference fringe (shown in the inset) corresponding to the radially polarized vortex beam. (d) Corresponding spatial distribution of the radial polarization state (solid white lines) retrieved using Eq. (C1).

In order to replicate the experimental situation, we consider generation of a radially polarized vortex beam in one arm of the interferometer by propagating linearly polarized light through a q -plate [19]. The resulting radially polarized vortex beam is subsequently passed through a quarter waveplate oriented at 45° with respect to the horizontal followed by a vertical linear polarizer. The corresponding expressions for the electric field can be obtained as

$$\begin{aligned} \mathbf{E}_1 &= E_0 \begin{pmatrix} 0 & 0 \\ 0 & 1 \end{pmatrix} \begin{pmatrix} 1+i & 1-i \\ 1-i & 1+i \end{pmatrix} \begin{pmatrix} \cos \varphi \\ \sin \varphi \end{pmatrix}, \\ E_0 &= \frac{\sqrt{2^{|l|+1}}}{2\omega_0 \sqrt{\pi |l|!}} \left(\frac{x + i \operatorname{sgn}(l)y}{\omega_0} \right)^{|l|} e^{-(x^2+y^2)/\omega_0^2}, \end{aligned} \quad (\text{C2})$$

where x and y are the transverse spatial coordinates, ω_0 is the spot size of the beam, l is the topological charge, and $\operatorname{sgn}(\cdot)$ is the sign function. The vertical polarization in the other arm

with a Gaussian profile can be written as

$$\mathbf{E}_2 = e^{-(x^2+y^2)/\omega_0^2} \begin{pmatrix} 0 \\ 1 \end{pmatrix}. \quad (\text{C3})$$

Once again, in order to simulate the experimental interference fringe pattern, we consider that \mathbf{E}_1 acquires a dynamical phase αy relative to \mathbf{E}_2 due to the path difference in the interferometer (α is the gradient of the dynamical phase along y). An arbitrary amplitude factor A is used in the electric field of amplitude of the reference arm of the interferometer to ensure comparable intensities in both the arms. The resultant electric field of interference is written as

$$\mathbf{E} = \mathbf{E}_1 e^{i\alpha y} + A\mathbf{E}_2. \quad (\text{C4})$$

In order to simulate the interference patterns, the following parameters were used: $\alpha = 0.075 \text{ rad } \mu\text{m}^{-1}$, $\omega_0 = 300 \text{ } \mu\text{m}$, and $l = 1$. The results of the simulation are summarized in Fig. 6, which demonstrates excellent recovery of the radial polarization distribution.

-
- [1] R. A. Chipman, *Handbook of Optics* (CRC, Boca Raton, 2003).
- [2] W. S. Bickel and W. M. Bailey, *Am. J. Phys.* **53**, 468 (1985).
- [3] N. Ghosh and A. I. Vitkin, *J. Biomed. Opt.* **16**, 110801 (2011).
- [4] J. Tinbergen, *Astronomical Polarimetry* (Cambridge University Press, Cambridge, 2005).
- [5] C. R. Kitchin, *Astrophysical Techniques* (CRC, Boca Raton, 2003).
- [6] J. Michl and E. W. Thulstrup, *Spectroscopy with Polarized Light: Solute Alignment by Photoselection in Liquid Crystals, Polymers and Membranes* (VCH, Weinheim, 1986).
- [7] N. Shitrit, I. Yulevich, E. Maguid, D. Ozeri, D. Veksler, V. Kleiner, and E. Hasman, *Science* **340**, 724 (2013).
- [8] R. Azzam, *Opt. Acta* **29**, 685 (1982).
- [9] D. Nandy, in *Subsurface and Atmospheric Influences on Solar Activity*, edited by R. Howe, R. W. Komm, K. S. Balasubramaniam, and G. J. D. Petrie (Astronomical Society of the Pacific, San Francisco, 2008), Vol. 383, p. 201.
- [10] R. A. Beth, *Phys. Rev.* **50**, 115 (1936).
- [11] L. Allen, M. W. Beijersbergen, R. J. C. Spreeuw, and J. P. Woerdman, *Phys. Rev. A* **45**, 8185 (1992).
- [12] H. He, M. E. J. Friese, N. R. Heckenberg, and H. Rubinsztein-Dunlop, *Phys. Rev. Lett.* **75**, 826 (1995).
- [13] V. S. Liberman and B. Y. Zel'dovich, *Phys. Rev. A* **46**, 5199 (1992).
- [14] K. Y. Bliokh, A. Aiello, and M. A. Alonso, in *The Angular Momentum of Light*, edited by D. L. Andrews and M. Babiker (Cambridge University Press, Cambridge, 2012), pp. 174–245.
- [15] X. Yin, Z. Ye, J. Rho, Y. Wang, and X. Zhang, *Science* **339**, 1405 (2013).
- [16] K. Y. Bliokh, F. J. Rodríguez-Fortuño, F. Nori, and A. V. Zayats, *Nat. Photon.* **9**, 796 (2015).
- [17] S. D. Gupta, N. Ghosh, and A. Banerjee, *Wave Optics: Basic Concepts and Contemporary Trends* (CRC, Boca Raton, 2015).
- [18] F. Tamburini, B. Thidé, G. Molina-Terriza, and G. Anzolin, *Nat. Phys.* **7**, 195 (2011).
- [19] L. Marrucci, C. Manzo, and D. Paparo, *Phys. Rev. Lett.* **96**, 163905 (2006).
- [20] S. Pancharatnam, *Proc. Indian Acad. Sci. A* **44**, 398 (1956).
- [21] M. V. Berry, *Proc. R. Soc. London Ser. A* **392**, 45 (1984).
- [22] R. Bhandari and J. Samuel, *Phys. Rev. Lett.* **60**, 1211 (1988).
- [23] K. Y. Bliokh, Y. Gorodetski, V. Kleiner, and E. Hasman, *Phys. Rev. Lett.* **101**, 030404 (2008).
- [24] X. Ling, X. Zhou, W. Shu, H. Luo, and S. Wen, *Sci. Rep.* **4**, 5557 (2014).
- [25] M. Berry, *Nature (London)* **326**, 277 (1987).
- [26] R. Simon, H. J. Kimble, and E. C. G. Sudarshan, *Phys. Rev. Lett.* **61**, 19 (1988).
- [27] E. Maguid, I. Yulevich, D. Veksler, V. Kleiner, M. L. Brongersma, and E. Hasman, *Science* **352**, 1202 (2016).
- [28] Q. Zhan and J. R. Leger, *Opt. Express* **10**, 324 (2002).
- [29] D. Kliger, J. Lewis, and C. Randall, *Elliptical Polarizers and Retarders in: Polarized Light in Optics and Spectroscopy* (Academic, New York, 1990).
- [30] C. Maurer, A. Jesacher, S. Fürhapter, S. Bernet, and M. Ritsch-Marte, *New J. Phys.* **9**, 78 (2007).
- [31] V. Duran, J. Lancis, E. Tajahuerce, and Z. Jaroszewicz, *J. Appl. Phys.* **97**, 043101 (2005).
- [32] M. Pal, C. Banerjee, S. Chandel, A. Bag, S. K. Majumder, and N. Ghosh, *Sci. Rep.* **6**, 39582 (2016).
- [33] M. V. Berry, *J. Mod. Opt.* **34**, 1401 (1987).
- [34] M. Takeda, H. Ina, and S. Kobayashi, *J. Opt. Soc. Am.* **72**, 156 (1982).
- [35] Q. Kemao, *Opt. Lasers Eng.* **45**, 304 (2007).
- [36] M. Servin, J. Marroquin, and F. Cuevas, *Appl. Opt.* **36**, 4540 (1997).